A method for resolving changes in atmospheric He/N_2 as an indicator of fossil fuel extraction and stratospheric circulation

Benjamin Birner[1], William Paplawsky[1], Jeffrey Severinghaus[1], and Ralph F. Keeling[1]

[1]Scripps Institution of Oceanography, UC San Diego, La Jolla, CA 92093, USA

Correspondence to: Benjamin Birner (bbirner@ucsd.edu)

Abstract. The atmospheric He/N_2 ratio is expected to be increasing due to the emission of He associated with fossil fuels and is expected to also vary in both space and time due to gravitational separation in the stratosphere. These signals may be useful indicators of fossil-fuel exploitation and variability in stratospheric circulation, but direct measurements of He/N_2 ratio are lacking on all time scales. Here we present a high-precision custom inlet system for mass spectrometers that continuously stabilizes the flow of gas during sample-standard comparison and removes all non-noble gases from the gas stream. This enables unprecedented accuracy in measurement of relative changes in the helium mole fraction, which can be directly related to the $^4He/N_2$ ratio using supplementary measurements of O_2/N_2, Ar/N_2 and CO_2. Repeat measurements of the same combination of high-pressure tanks using our inlet system achieves a He/N_2 reproducibility of ~10 per meg (i.e. 0.001%) in 6–8h analyses. This compares to interannual changes of gravitational enrichment at ~35 km in the mid latitude stratosphere of order 300–400 per meg, and an annual tropospheric increase from human fossil fuel activity of less than ~30 per meg y^{-1} (bounded by previous work on helium isotopes). The gettering and flow-stabilizing inlet may also be used for the analysis of other noble gas isotopes and could resolve previously unobserved seasonal cycles in Kr/N_2 and Xe/N_2.

1 Introduction

The atmospheric mole fraction of helium in dry air is typically ~5.24 ppm (Glückauf, 1944) with an isotopic abundance of ^4He about 10^6 times greater than ^3He. On geological time scales, the natural concentration of ^4He in the atmosphere is set by a balance of ^4He loss to space and ^4He release from the Earth's crust, where it is produced by radioactive decay of uranium and thorium (Kockarts, 1973; Pierson-Wickmann et al., 2001; Sano et al., 2013; Torgersen, 1989; Zartman et al., 1961). Over the past century, human exploitation of fossil fuels likely has accelerated the release of crustal He (Boucher et al., 2018c; Lupton and Evans, 2013, 2004; Mabry et al., 2015; Oliver et al., 1984; Pierson-Wickmann et al., 2001; Sano et al., 1989), but direct observations of a secular increase of atmospheric ^4He are lacking. Additionally, recent measurements and model simulations reveal a small depletion of heavy gas argon in the stratosphere by gravitational separation (Belikov et al., 2019; Birner et al., 2020; Ishidoya et al., 2020, 2018, 2013, 2008; Sugawara et al., 2018) suggesting a corresponding enrichment of the light gas helium. Gravitational separation is only partially counteracted by the large-scale stratospheric circulation and mixing, which

tends to homogenize the atmosphere. Variability in stratospheric circulation and stratosphere-troposphere exchange (STE) could therefore impact the degree of fractionation and cause additional interannual changes in the stratospheric and, to a much lesser extent, the tropospheric abundance of ^{4}He.

Measurements of He/N_2 may provide an alternative indicator of variations in stratospheric circulation and STE. An improved understanding of STE is critical because stratospheric circulation changes affect tropospheric trends of societally-important greenhouse gases and geochemical tracers such as N_2O, CH_4, ^{14}C, O_3 and CFCs (Arblaster et al., 2014; Graven et al., 2012; Hamilton and Fan, 2000; Hegglin and Shepherd, 2009; Montzka et al., 2018; Nevison et al., 2011; Simmonds et al., 2013). These gases all have significant sources or sinks in the stratosphere that cause strong stratosphere-troposphere concentration differences. Global circulation models consistently predict an acceleration of the stratospheric Brewer-Dobson Circulation (BDC; Brewer, 1949; Dobson, 1956) under global warming (Butchart, 2014). Stratospheric circulation is also naturally modulated on a range of shorter time scales from synoptic-scale events to decadal variations (e.g., Holton et al., 1995; Li et al., 2012; Flury et al., 2013; Butchart, 2014; Ray et al., 2014). Circulation changes have typically been observed using measurements of numerous different trace gases in the stratosphere (e.g., CO_2, SF_6, H_2O, O_3, CO, or N_2O) (e.g., Bönisch et al., 2009; Engel et al., 2009, 2017; Ray et al., 2010; Haenel et al., 2015). However, interpretation of these tracers of stratospheric circulation is complicated by complex chemical sources, sinks and tropospheric histories, whereas gravitational fractionation of He/N_2 is governed by comparatively simple physics and expected to increase smoothly in the troposphere.

Atmospheric He/N_2 measurements may also provide an indication of the history of fossil-fuel usage. Previous attempts to measure the fossil-fuel signal in He have centered on measurements of changes in the atmospheric ^{3}He/^{4}He isotope ratio typically using multicollector, static vacuum mass spectrometers (Boucher et al., 2018c; Lupton and Evans, 2013, 2004; Mabry et al., 2015; Oliver et al., 1984; Sano et al., 1989). However, measurements of the ^{3}He/^{4}He ratio are fundamentally limited by the extremely low abundance of ^{3}He (e.g., Mabry et al., 2015; Boucher et al., 2018b), with only about 1 in 730,000 He atoms being ^{3}He. Therefore, the precision on individual ^{3}He/^{4}He analyses is currently limited to ~±0.2% (2σ). This is insufficient for the detection of the stratospheric and anthropogenic signals we are interested in, and which we estimate to cause variations in the atmospheric ^{4}He abundance on the order of 0.0030 to 0.04% y^{-1} (see section 2.1 & 2.2.). Moreover, small changes in ^{3}He from radioactive decay of tritium in nuclear warheads may complicate the interpretation of ^{3}He/^{4}He results (e.g., Boucher et al., 2018c; Lupton and Evans, 2004).

Thus far, the most promising direct measurements of the atmospheric ^{4}He mixing ratio were produced by Holland and Emerson (1987). Holland and Emerson repeatedly introduced sample and standard air into a mass spectrometer through a charcoal trap to concentrate helium. However, their method also only achieved an instrument precision of 0.22% (2σ) and is thus not suitable for the science discussed above.

Here we describe a method to measure relative differences in ^{4}He mole fraction (^{4}He/M) between two large samples of air using a custom mass spectrometer inlet system. The helium mole fraction can later be mathematically translated to our target ratio, ^{4}He/N_2, given supplementary measurements of O_2, Ar, and CO_2 (see discussion). This is advantageous because N_2 is near-constant in the atmosphere making ^{4}He/N_2 more readily interpretable than ^{4}He/M. The ^{4}He/M method depends on

stabilization of the air flow to the ion source between a sample and standard gas to achieve high precision differencing. Novel elements in our setup include continuous-flow removal of reactive gases via titanium gettering immediately upstream of the mass spectrometer inlet, and the use of an actively-controlled open split (Henneberg et al., 1975) for balancing pressures upstream of a shared capillary directed towards the mass spectrometer. Gas handling techniques, the inlet system and the continuous-flow getter oven are described in detail below.

1.1 Gravitational fractionation of He/N_2 in the stratosphere

The notion that the stratospheric and tropospheric He/N_2 ratio must vary in response to fluctuations in stratospheric circulation is based on studies of the atmospheric Ar/N_2 ratio (Birner et al., 2020; Ishidoya et al., 2020). Relative changes in the Ar/N_2 ratio (or He/N_2) are commonly expressed in delta notation:

$$\delta(Ar/N_2) = \frac{\left(\frac{Ar}{N_2}\right)_{SA}}{\left(\frac{Ar}{N_2}\right)_{ST}} - 1 \qquad (1)$$

where subscripts SA and ST refer to the ratio in a sample and a standard gas mixture, respectively. δ(Ar/N_2) is multiplied by 10^6 and expressed in "per meg" units.

Sensitivity tests with the 2-D chemical-dynamical-radiative model of the atmosphere SOCRATES by Ishidoya et al. (2020) indicate that significant temporal changes in stratospheric Ar/N_2 should occur in response to an acceleration or deceleration of the BDC. The simulations also suggest a weak stratospheric influence on tropospheric Ar/N_2. Ishidoya et al find that imposing a gradual acceleration of the BDC of 4% dec^{-1} leads to a 40 per meg dec^{-1} increase in δ(Ar/N_2) at ~35 km altitude in northern mid-latitudes, and a corresponding 1.3 per meg dec^{-1} decrease of δ(Ar/N_2) in the troposphere. Furthermore, they find that imposing 3-year periodic changes of 10% in BDC yields anomalies of ±25 and ±0.4 per meg in stratospheric and tropospheric δ(Ar/N_2), respectively. Tropospheric observations of δ(Ar/N_2) by Ishidoya et al. (2020) would be consistent with larger STE-induced interannual changes of tropospheric Ar/N_2. Variability of the BDC on the order of 10% or more on seasonal to decadal time scales is consistent with published estimates (Flury et al., 2013; Ray et al., 2014; Salby and Callaghan, 2006).

The atmospheric He/N_2 ratio must be more strongly impacted by gravitational fractionation than Ar/N_2 due to the larger mass difference and higher diffusivity of He than Ar, which brings He closer to gravitational equilibrium. The gravitational fractionation effect on He/N_2 can be scaled from Ar/N_2 (Birner et al., 2020) using the molar mass difference to air ΔM_i ($\Delta M_i = M_i - 0.02896$ kg mol^{-1}) and the molecular diffusivity D_i of gas i in air as:

$$\delta\left(\frac{\mathrm{He}}{\mathrm{N_2}}\right) = \frac{\left(\frac{He}{N_2}\right)_{SA}}{\left(\frac{He}{N_2}\right)_{ST}} - 1 \approx \frac{D_{He}^{air}\Delta M_{He} - D_{N2}^{air}\Delta M_{N2}}{D_{Ar}^{air}\Delta M_{Ar} - D_{N2}^{air}\Delta M_{N2}}\delta(\mathrm{Ar/N_2}). \qquad (2)$$

Using the Fuller method (Reid et al., 1987), D_{He}^{air} is 3.6 (3.5) times greater than D_{Ar}^{air} (D_{N2}^{air}), and ΔM_{He} is more than twice as large and opposite sign than ΔM_{Ar} ($\Delta M_{He} = -0.02496, \Delta M_{Ar} = 0.01102, \Delta M_{N2} = -0.0009466$). This makes $\delta(He/N_2)$ ~-7.5 times more strongly fractionated by gravity than $\delta(Ar/N_2)$ in the stratosphere but in opposite direction.

1.2 Other controls on tropospheric He/N_2

A variety of known natural processes influence tropospheric $^4He/N_2$ is summarized in Figure 1 and Table 1. Natural ^4He release from the Earth's crust is mediated by volcanism, ground water discharge and diffusive leakage. At the same time, helium is lost to space by thermal and non-thermal escape (Kockarts, 1973; Oliver et al., 1984; Pierson-Wickmann et al., 2001; Sano et al., 2013; Torgersen, 1989). Based on these natural fluxes and the total atmospheric burden, the atmospheric residence time of ^4He is estimated to be ~1 million years.

Over the few last centuries, He release from fossil-fuel extraction has dwarfed the natural release rates of ^4He by several orders of magnitude. Based on knowledge of fossil fuel usage and He content of the material (Table 1) the additional ^4He release rate is estimated to be of order 3 to 30×10^{10} mol yr^{-1} (e.g., Oliver et al., 1984; Sano et al., 1989, 2013; Pierson-Wickmann et al., 2001) implying that $^3He/^4He$ should be decreasing at rates between 35 and 350 per meg y^{-1}. However, in contrast to these predictions and some earlier observations (Oliver et al., 1984; Pierson-Wickmann et al., 2001; Sano et al., 2010, 1989), no significant trend in atmospheric $^3He/^4He$ has been observed using archived air samples spanning from the beginning of the 20th century to today. These more recent observations bound any trend in $^3He/^4He$ to within roughly ±30 per meg per year (2σ), suggesting similarly small increase rates in $\delta(He/N_2)$ (Boucher et al., 2018c; Lupton and Evans, 2013, 2004; Mabry et al., 2015).

He release from fossil-fuel extraction is also expected to impose an interhemispheric gradient in $\delta(He/N_2)$. A rough upper bound can be estimated by assuming all fossil-fuel derived He emissions occur in the Northern Hemisphere and interhemispheric mixing of the atmosphere has a time scale of about one year. This would yield a north-south difference of 30 per meg, equal to the expected annual rise in $\delta(He/N_2)$.

Seasonal and long-term ocean warming can cause small changes in He/N_2, mainly due to the impact on N_2. From observations of $\delta(Ar/N_2)$ (Keeling et al., 2004) and solubility data of Ar, He and N_2 (Hamme and Emerson, 2004; Weiss, 1971), we estimate that the impact on He/N_2 of air-sea exchanges is on the order of 0.16 per meg y^{-1} for the secular ocean warming trend and 3-9 per meg for seasonal heat exchanges. Therefore, the ratio of stratospheric signals to ocean warming is ~12 times greater for He/N_2 than Ar/N_2 and the effect of slow ocean warming is over two orders of magnitude smaller than the influence of fossil fuel exploitation.

The He/N_2 ratio could also be impacted by processes changing atmospheric N_2. However, the annual removal of $7.5x10^{12}$ mol N_2 y^{-1} by anthropogenic nitrogen fixation in agriculture, combustion, and industry is clearly negligible compared to the ~$1.4x10^{20}$ moles of N_2 in the whole atmosphere (Fowler et al., 2013). Volcanic emissions of N_2 are likewise negligible, on the order of 10^9 mol y^{-1}.

2 Methods

Our He/N_2 analysis method relies on measuring the helium mole fraction relative difference between an air sample and a standard gas using a single collector for $^4He^+$ on a magnetic sector mass spectrometer (MS). Crucially, whole dry air is pressure-stabilized to a high level prior to gettering, so that the beam intensity ratio being measured is effectively the ^4He to air ratio. Measurements of the He mole fraction difference can also be expressed similarly to Eq. (1) as $\delta(^4He/M)$ where M is total moles. By applying small corrections for variations in O_2/N_2, Ar/N_2, and CO_2, the quantity $\delta(^4He/M)$ is easily related to $\delta(^4He/N_2)$.

The MS is interfaced to a custom inlet system with on-line gettering and active flow stabilization using an actively pressure-controlled open split (Henneberg et al., 1975), as shown in Figure 2.

2.1 The Inlet system

The design of the inlet system incorporates elements of an open split (Henneberg et al., 1975) but further stabilizes the pressure using active control elements and allows active switching between a sample (SA) and reference standard gas stream (ST). Pneumatically-actuated pistons (B in Fig. 2) alternately slide 0.3-mm tubes exhausting sample or standard gas close to a shared intake capillary, which is placed at the end of the stabilization chamber (C in Fig. 2) and connects the chamber to the getter oven and MS. Air actuation of the pistons is controlled by the MS through an electronic valve assembly (Clippard, model: EMS-08). The flexible 0.3mm tubes are mounted leak-tight inside sturdier 1/16" OD tubing which is fixed to the piston and moved with a stroke length of 7 cm. A sliding seal is made between 1/8" OD outer tubing and the 1/16" OD tubing using a compressed O-ring lubricated with TorrLube vacuum grease. This setup creates a movable feedthrough port for the 0.3-mm tubes containing sample and standard gas and the pressure stabilization chamber, thus allowing the chamber to be operated at a selected pressure above or below ambient. The default setting is 14 psia (96.5 kPa).The chamber is shaped as a funnel to guide the sliding tubing into a reproducible resting position. Variations in chamber pressure are measured with a 0.2-Torr MKS 223B differential pressure gauge and are limited to better than 1 part in 10^6 by opening an MKS Type 248 Control Valve, which allows most of the gas in the stabilization chamber to be pumped away by a vacuum pump. The valve is controlled via an MKS 250E Control Module. The shared outlet capillary from the pressure-stabilization chamber is crimped and thermally insulated to avoid changes in conductance and thus air flow caused by room temperature fluctuations. The pressure in the getter oven (D in Fig. 2) is about 2 mTorr (0.3 Pa) because the getter material effectively acts as a vacuum pump.

2.2 Continuous-flow gettering

In the getter chamber (D in Fig. 2), 99.9% pure titanium sponge (Ti) irreversibly reacts with N_2, O_2, CO_2, and other non-noble gases in air to form titanium nitride (TiN), titanium dioxide (TiO_2), titanium carbide (TiC) and other compounds at ~850°C. This increases the concentration of He in the gas mixture by a factor of about 100, boosting precision. The getter oven has an inner diameter of 0.94 cm and a length of 22.5 cm. It is manufactured from heat resistant stainless steel (SS310) and equipped

with VCR face seals for easy maintenance. The temperature of the getter oven is determined by manually adjusting the power provided to two OMEGA CRWS semi-cylindrical heaters surrounding the getter. The heaters are additionally equipped with an independent limit controller for safety.

The gettering efficiency depends on the heaters' temperature and must be balanced against material tolerance and increased evolution of H_2 gas from the metal in the getter. H_2 forms a solid solution in Ti and is continuously released to the gas stream when Ti is heated. The solution process is reversible and H_2 is absorbed if the Ti is cooled down. H_2 could interact with He^+ in the source or combine with ionized gas to form hydride compounds such as ArH^+ (Fig. 3) However, since the H_2 flux into the gas stream varies slowly compared to the 30-second timescale of switching between sample and standard gas, the impact of H^+ cancels during sample-standard comparison. In its current size (~10–12 g Ti), the getter can be used for 70–80h before the Ti must be replaced to prevent N_2 breakthrough. This requires breaking vacuum in the inlet approximately once every four weeks depending on usage. After replacement, fresh titanium is gradually heated to 900°C over ~12h in isolation from the MS to allow degassing without contaminating the MS. A coarse mesh of metal wire and 2µm SWAGELOK filters on both sides of the getter prevent getter-derived dust from entering the vacuum system and MS.

2.3 Inlet operation

We have developed customized scripts using the software ISODAT provided with any MAT253 mass spectrometer to control the inlet system and operate the pneumatic actuators for He/M analysis (Fig. 3). In a typical run, the instrument performs sample-standard gas switching with a ~30 second switching time (~60 sec full cycle), using a conservative 18-second idle time to allowing the MS signal to stabilize before integration . As customary in dynamic MS noble gas application, we group each analysis into blocks consisting of (i) adjusting the accelerating voltage to find the center of the ^4He peak followed by (ii) 20 sample-standard comparisons. Background concentrations of ^4He in the MS are determined by closing the inlet upstream of the getter oven and subtracted daily. Data are quality controlled and anomalous cycles are rejected when delta values deviate by more than 3 standard deviations from the smoothed time series or when there are abrupt changes detected in the ion beam associated with instability in the MS source (not shown). ISODAT also monitors the MS source pressure and closes the external change-over-valve (Fig. 2) to protect the MS in case of a pressure control failure.

2.4 Gas handling and sample delivery systems

Air is delivered to the inlet system from a pair of high-pressure gas cylinders (A in Fig. 2). For He/N_2 standard gas, we rely on compressed dry air stored in high-pressure cylinders, as is conventional for atmospheric measurements of O_2/N_2, CO_2, and Ar/N_2 (Keeling et al., 2007). All cylinders are stored horizontally for 2 days in a thermal enclosure at ambient temperature before analysis to minimize the risk of thermal fractionation. The pressure is dropped to slightly above ambient directly at the head valve of high-pressure cylinders using capillaries rather than regulators. The use of capillaries ensures that all wetted parts are exclusively metal, which is impermeable to He, and eliminates problems we encountered using regulators during initial tests. Due to the use of capillaries, the gas delivery system cannot be evacuated efficiently and instead must be purged

for several hours ahead of analysis until the signal stabilizes. The flow rates in the lines are monitored using 0.1 liter per minute Omron DF6-P flow meters and are manually balanced at around 27-28 cm^3 min^{-1} before every analysis by adjusting the crimping of both 316 stainless steel capillaries. Sample and standard gas streams are both dried before entering the pressure stabilization chamber (C in Fig. 2) by flowing through U-shaped cold traps made from about 25 cm of 1/4" stainless steel tubing. The traps are held at about -80°C by submerging the metal tubing in a dry ice and ethanol mixture for the duration of the analysis.

2.5 Converting δ(He/M) to δ(He/N_2)

δ(He/M) can be related to δ(He/N_2) using

$$\delta(He/N_2) \simeq \delta(He/\mathrm{M}) + \delta(O_2/N_2)X_{O_2} + \delta(Ar/N_2)X_{Ar} + dX_{CO_2} \quad (3)$$

as derived in Box 1, using independent measurements of δ(O_2/N_2), δ(Ar/N_2), and dX_{CO2} (Keeling et al., 2004, 1998). These corrections are relatively small and therefore do not significantly contribute to the overall uncertainty of δ(He/N_2). Analytical uncertainty for measurements of δ(O_2/N_2), δ(Ar/N_2), and dX_{CO2} is typically better than 1.5 per meg , 11 per meg, and 0.2 ppm (Keeling et al., 1998, 2004), yielding uncertainties of 0.3, 0.11 and 0.2 per meg in the terms $\delta\left(\frac{O_2}{N_2}\right)X_{O_2}$, $\delta(Ar/N_2)X_{Ar}$, and dX_{CO_2}. The long-term atmospheric changes in δ(O_2/N_2) ~ -19 per meg yr^{-1} and dX_{CO2} ~2.5 ppm yr^{-1} yield corrections of approximately -4 per meg yr^{-1} and +2.5 per meg yr^{-1}, respectively. The seasonal variations in δ(O_2/N_2)X_{O2} and dX_{CO2} partly cancel, yielding net seasonal corrections of ~10 per meg in both hemispheres. The term δ(Ar/N_2)X_{Ar} contributes variations less than 1 per meg on all time scales.

Box 1. Deriving the helium-to-nitrogen ratio from δ(He/M)

A relationship between δ(He/N_2) and δ(He/M) can be derived from:

$$\delta(He/N_2) = \frac{dHe}{He} - \frac{dN_2}{N_2} = \frac{dHe}{He} - \frac{dM}{M} - \frac{dN_2}{N_2} + \frac{dM}{M} = \delta(He/\mathrm{M}) - \frac{dN_2}{N_2} + \frac{dN_2 + dO_2 + dAr + dCO_2}{M}$$

Using $\frac{dN_2}{\mathrm{M}} = \frac{dN_2}{N_2} X_{N_2}$, $\frac{dO_2}{\mathrm{M}} = \frac{dO_2}{O_2} X_{O_2}$, etc, where X_{i} is the mole fraction of gas i, yields

$$\delta(He/N_2) = \delta(He/\mathrm{M}) + \frac{dN_2}{N_2}\left[-1 + X_{N_2} + X_{O_2} + X_{Ar} + X_{CO_2} + X_{H_2O} \ldots\right] + \left[\frac{dO_2}{O_2} - \frac{dN_2}{N_2}\right]X_{O_2} + \left[\frac{dAr}{Ar} - \frac{dN_2}{N_2}\right]X_{Ar} + \left[\frac{dCO_2}{CO_2} - \frac{dN_2}{N_2}\right]X_{CO_2} + \cdots$$

This can be simplified to Eq. (3) using $\left[\frac{dCO_2}{CO_2} - \frac{dN_2}{N_2}\right]X_{CO_2} = dX_{CO_2}$, which follows because relative changes in CO_2 are much larger than relative changes in N_2.

3 Results

3.1 Gettering performance

A mass scan of air introduced through the gettering and flow-stabilizing inlet system revealed that N_2 and O_2 are almost completely removed from the air by the on-line getter (Fig. 4). He is effectively preconcentrated in the gas mixture. ^{40}Ar ions with one or more charges yield the largest beams in the scan followed by ^{36}Ar, and H_2 evolving from the hot metal in the getter oven.

3.2 Response time

Our setup demonstrates the ability to transition between sample and standard gas with an e-folding time scale of ~4 seconds (Fig. 5). The e-folding time is primarily controlled by the volume of the getter and the total flow of gas through the getter. Regions of the inlet system upstream of the getter experience ~100x faster flushing than downstream of the getter because the gas upstream still contains N_2 and O_2 and hence flows much faster. An associated large drop in pressure however ensures that all parts of the inlet system are flushed out similarly quickly. The e-folding time does not change substantially over the life span of the getter.

3.3 Analytical precision

Using the default 60 sec sample-standard cycle, the gettering and flow-stabilizing inlet system achieves an internal precision in δ(He/M) of approximately ±15 per meg over 1.5h and ±8 per meg for samples run 6h or longer (1σ, standard error of ~90 and ~360 cycles respectively). The (external) reproducibility of repeated 6–8h measurements of the same sample and standard gas cylinder combination is comparable and essentially as expected from the shot-noise on the ^4He ion current (Figs. 6&7).

The zero enrichment, i.e., the delta value observed when introducing the same gas through sample and standard side of the inlet, is generally small and stable over time. It is tested by mounting the crimped delivery capillaries (A in Fig. 2) to a tee fitting, which splits the gas stream at high pressure from a single tank of air. This tee minimizes thermal fractionation by dividing the flow at a junction machined into the center of a large brass block (Keeling, 1988). Identical delta values (within error) obtained after reversing the outlet from the tee demonstrate that no measurable fractionation occurs within the tee and therefore that the zero enrichment reflects a persistent asymmetry somewhere downstream, most likely within the pressure stabilization chamber. The typical zero enrichment varies slightly with the mean flow of gas into the stabilization chamber (F), the pressure in the chamber (P), and the flow offset between SA and ST side (ΔF) before entering the stabilization chamber (Fig. 7). Weighted multiple linear regression analysis using 3 different pressure levels (9 psi, 14 psi, and 16 psi, i.e, 62.1, 96.5, and 110.3 kPa) and predictors F, P, and ΔF reveals that the zero enrichment value decreases by 2.8±0.9 per meg per 1 cm^3 min^{-1} change in mean flow away from 27.5 cm^3 min^{-1} and increases by 17.2±4.8 per meg per 1 cm^3 min^{-1} flow imbalance between SA and ST (1σ). The analysis also finds that the dependence of δ(He/M) on F and ΔF is significant at the 5% level. For a balanced flow of 27.5 cm^3 min^{-1} and a pressure of 62.1, 96.5 and 110.3 kPa in the stabilization chamber, the mean zero

enrichment is -9.61±7.2, 1±3.7, and -15.7±4.7 per meg, respectively. For actual measurements, P is held constant at 96.5 kPa with very high precision. F and ΔF are stable over 8h to within ±0.2 cm^3 min^{-1}. This typically yields a correction for mean gas flow and flow imbalance of less than 10 per meg with an uncertainty smaller than 6 per meg, which increases the overall analytical uncertainty in repeat tank analysis from 8 to 10 per meg.

4 Discussion

The gettering and flow-stabilizing inlet system has demonstrated the ability to determine the helium mole fraction difference between a sample and standard gas, δ(He/M), to about 10 per meg in a single 6–8h analysis and has a range of possible applications. Our primary targets are (i) to use stratospheric δ(He/N_2) as a tracer of the large-scale stratospheric circulation and (ii) to evaluate tropospheric δ(He/N_2) trends as a possible indicator of anthropogenic fossil fuel exploitation.

We expect an excellent signal-to-noise ratio for the detection of stratospheric changes in δ(He/N_2). Interannual variability in stratospheric δ(He/N_2) is likely on the order 300–400 per meg (Table 1). Repeat 6–8h measurements of a high-pressure cylinder currently achieve a precision of ~10 per meg, or about 40 times less than the stratospheric signal. Associated changes in tropospheric δ(He/N_2), in contrast, are likely much smaller at around 6 per meg and therefore at or below the current limit of detection even after averaging of multiple samples.

Tropospheric He/N_2 measurements can help quantify the anthropogenic ^{4}He release over time due to fossil fuel extraction (Boucher et al., 2018c; Lupton and Evans, 2013, 2004; Mabry et al., 2015; Oliver et al., 1984; Sano et al., 2010, 1989). Although theoretical predictions clearly support an anthropogenic ^{4}He increase, past observational studies produced conflicting evidence. Recent improvements in analytical methods and sampling have narrowed the uncertainty in ^{3}He/^{4}He trend estimates to <30 per meg y^{-1} with a mean statistically indistinguishable from zero (Table 1). However, with a precision of ~10 per meg on single samples, measurements of δ(^{4}He/N_2) on decades-old archived air may allow trend detection to ~1 per meg y^{-1} or better, while also avoiding possible complications from ^{3}He emissions that could bias estimates of the ^{4}He source from ^{3}He/^{4}He. Another possible application is the investigation of spatial gradients in atmospheric δ(He/N_2) caused by the distribution of local volcanic or anthropogenic sources (e.g., Sano et al., 2010; Boucher et al., 2018c). High precision δ(He/N_2) may allow the detection of diffuse helium release in regions of volcanic activity (Boucher et al., 2018b). Furthermore, global north-south δ(He/N_2) gradients from anthropogenic emission sources concentrated in the Northern Hemisphere are likely on the order of 10s of per meg and thus may also be detectable directly. Alternatively, studies could target more local gradients around oil or natural gas facilities that are likely even greater.

The method developed here is potentially applicable to measure the abundance of any noble gas in air. The intensity of the ion beam and thus the precision for different noble gases depends on their natural abundance and ionization efficiency in the MS source. ^{20}Ne and ^{22}Ne have isobaric interferences from doubly charged Ar and CO_2, but Kr and Xe yield usable ion beams (Table 2). We estimate a precision of ~5 and ~19 per meg for repeat 6–8h analyses of δ(^{84}Kr/$^{28}N_2$) and δ(^{129}Xe/$^{28}N_2$) respectively, by assuming that precision scales with the square root of the total ions counted as expected from shot-noise

behavior. This estimate compares favorably to the precision currently reported in conventional dual inlet mass spectrometry studies (Baggenstos et al., 2019; Bereiter et al., 2018). For example, Baggenstos et al. (2019) achieved a precision of 88 per meg and 203 per meg for repeat ~2h analyses of $\delta(^{84}Kr/^{40}Ar)$ and $\delta(^{132}Xe/^{40}Ar)$ in ambient air, respectively.

The improved precision enabled by our inlet system should be sufficient to resolve the previously unobserved annual cycle of Kr and Xe caused by the seasonal release and uptake of both gases by the ocean as it warms and cools. The seasonal cycle of $\delta(^{40}Ar/^{28}N_2)$ has an amplitude of 5–15 per meg in the extratropics (Keeling et al., 2004). $\delta(^{84}Kr/^{28}N_2)$ and $\delta(^{132}Xe/^{28}N_2)$ however are ~3.4 and ~8.9 times more sensitive than $\delta(^{40}Ar/^{28}N_2)$ to changes in ocean temperature owing to the different temperature-dependences of Ar, Kr and Xe solubility in seawater (Hamme and Emerson, 2004; Jenkins et al., 2019). This implies that seasonal variations in $\delta(^{84}Kr/^{28}N_2)$ and $\delta(^{132}Xe/^{28}N_2)$ have a magnitude of 17–51 and 45–134 per meg respectively, which would be readily resolved if precision of our system scales as expected with signal strength.

The gettering inlet and MS system was applied here only for single ion (He^+) detection, but alternately could be applied for multi-ion collection. The acquisition of Kr and Xe isotope ratios for example would provide valuable additional information for detecting artifactual fractionation during sampling and allow further improvements in precision by increasing the total number of ions collected.

The need for only a single ion detector also allows the gettering and flow-stabilizing inlet to be interfaced with simpler and more affordable mass spectrometers, such as quadrupole systems. The performance of the system will depend on the stability of the $^4He^+$-ion beam over the time scale of switching and will need to be evaluated critically, but any variability on time scales longer than the switching time is canceled by sample-standard differencing.

Additional work is needed to further improve calibration methods and to establish standard procedures for collecting air samples while avoiding artifacts in He/N_2 at the 10 per meg level. We currently need samples of ~16-20l for a full 8h analysis because long purging and analysis times are necessary to achieve a precision of 10 per meg. If reduced precision is acceptable, analyses time can be shortened but purging of the inlet system for at least one hour is needed before each analysis even for lower precision work. Furthermore, air samples must currently be provided at pressure greater than 3 atm to allow sufficient flow through the narrow tubing into the pressure-stabilization chamber. The reproducibility of measurements also depends on adequate calibration strategies. The short-term reproducibility of high-pressure cylinders shown in Figure 6 and the long-term stability established for O_2/N_2, CO_2, and Ar/N_2 standard gases in previous work (Keeling et al., 2007) suggest that long-term stability in $\delta(He/N_2)$ is achievable but needs further evaluation.

5 Conclusions

Here, we present a new method for high-precision measurements of changes in the ^4He mole fraction of atmospheric air which can be directly related to changes in He/N_2 ratio. The method relies on monitoring of the $^4He^+$ ion beam in a mass spectrometer during sample-standard switching. The ion beam is stabilized by flowing sample and standard air through a single capillary into the MS from an actively pressure-controlled open-split (Henneberg et al., 1975), such that variability of the $^4He^+$ ion beam

directly reflects differences in the helium mole fraction of the gas mixtures. Measurements of the helium mole fraction can easily be converted to $\delta(He/N_2)$ if O_2/N_2, Ar/N_2, and CO_2 concentrations of the sample are determined as well. An online getter preconcentrates He and other noble gases before entry into the MS by chemically removing >99.99% of all N_2 and O_2 in a reaction with titanium sponge. Our method thereby avoids the need for peak jumping and a multi-collector mass spectrometer, while achieving a precision of ~10 per meg (1σ) on repeat analysis of $\delta(He/N_2)$ in high-pressure tanks of air.

In future work, the gettering and flow-stabilizing inlet system could be used to investigate possible interannual to decadal changes in stratospheric $\delta(He/N_2)$ linked to variability in stratospheric circulation and stratosphere-troposphere exchange processes. Additional applications could include the search for a signal of anthropogenic helium release during fossil fuel extraction and burning, or measurements of spatial gradients resulting from localized human or natural sources of helium. The setup is also suitable for the analysis of other noble gases and could therefore be used to study seasonal ocean warming associated with degassing or uptake of Kr and Xe from the ocean (Baggenstos et al., 2019; Bereiter et al., 2018).

6 Acknowledgements

We thank Ross Beaudette, Alan Seltzer, Sarah Shackleton, Jacob Morgen, Jessica Ng, and Eric Morgan for laboratory support and insightful discussions during the development of the He/N_2 analysis system. We are grateful to Shane Clark, Savannah Hatley, Adam Cox, and Timothy Lueker for providing high-pressure cylinders used during testing. We also thank them for maintaining and operating the Ar/N_2, O_2/N_2 and CO_2 analysis systems in the Keeling laboratory. This work was supported by the National Science Foundation grants MRI-1920369 and AGS-1940361.

7 Data availability

Data presented in this manuscript are available as an electronic supplement to this paper from the journal website.

8 Competing interests

The authors declare that they have no conflict of interest.

9 Author contribution

BB designed and build the inlet system with important design expertise from WP, JS and RK. BB performed all testing and prepared the manuscript with contributions from all co-authors.

10 References

Arblaster, J.M., Gillett, N.P., Calvo, N., Forster, P.M., Polvani, L.M., Son, S.-W., Waugh, D.W., Young, P.J., 2014. Stratospheric ozone changes and climate, Chapter 4, Scientific Assessment of Ozone Depletion: 2014, Global Ozone Research and Monitoring Project – Report No. 55. Geneva, Switzerland.

Baggenstos, D., Häberli, M., Schmitt, J., Shackleton, S.A., Birner, B., Severinghaus, J.P., Kellerhals, T., Fischer, H., 2019. Earth's radiative imbalance from the Last Glacial Maximum to the present. Proc. Natl. Acad. Sci. U. S. A. 116, 14881–14886. https://doi.org/10.1073/pnas.1905447116

Belikov, D., Sugawara, S., Ishidoya, S., Hasebe, F., Maksyutov, S., Aoki, S., Morimoto, S., Nakazawa, T., 2019. Three-dimensional simulation of stratospheric gravitational separation using the NIES global atmospheric tracer transport model. Atmos. Chem. Phys. 19, 5349–5361. https://doi.org/10.5194/acp-19-5349-2019

Bereiter, B., Shackleton, S., Baggenstos, D., Kawamura, K., Severinghaus, J., 2018. Mean global ocean temperatures during the last glacial transition. Nature 553, 39–44. https://doi.org/10.1038/nature25152

Birner, B., Chipperfield, M.P., Morgan, E.J., Stephens, B.B., Linz, M., Feng, W., Wilson, C., Bent, J.D., Wofsy, S.C., Severinghaus, J., Keeling, R.F., 2020. Gravitational separation of Ar/N_2 and age of air in the lowermost stratosphere in airborne observations and a chemical transport model. Atmos. Chem. Phys. Discuss. 1–34. https://doi.org/10.5194/acp-2020-95

Bönisch, H., Engel, A., Curtius, J., Birner, T., Hoor, P., 2009. Quantifying transport into the lowermost stratosphere using simultaneous in-situ measurements of SF_6 and CO_2. Atmos. Chem. Phys. 9, 5905–5919. https://doi.org/10.5194/acp-9-5905-2009

Boucher, C., Lan, T., Mabry, J., Bekaert, D. V., Burnard, P.G., Marty, B., 2018a. Spatial analysis of the atmospheric helium isotopic composition: Geochemical and environmental implications. Geochim. Cosmochim. Acta 237, 120–130. https://doi.org/10.1016/j.gca.2018.06.010

Boucher, C., Lan, T., Marty, B., Burnard, P.G., Fischer, T.P., Ayalew, D., Mabry, J., Maarten de Moor, J., Zelenski, M.E., Zimmermann, L., 2018b. Atmospheric helium isotope composition as a tracer of volcanic emissions: A case study of Erta Ale volcano, Ethiopia. Chem. Geol. 480, 3–11. https://doi.org/10.1016/j.chemgeo.2017.05.011

Boucher, C., Marty, B., Zimmermann, L., Langenfelds, R., 2018c. Atmospheric helium isotopic ratio from 1910 to 2016 recorded in stainless steel containers. Geochemical Perspect. Lett. 6, 23–27. https://doi.org/10.7185/geochemlet.1804

Brewer, A.W., 1949. Evidence for a world circulation provided by the measurements of helium and water vapour distribution in the stratosphere. Q. J. R. Meteorol. Soc. 75, 351–363. https://doi.org/10.1002/qj.49707532603

Butchart, N., 2014. The Brewer-Dobson circulation. Rev. Geophys. 52, 157–184. https://doi.org/10.1002/2013RG000448

Dobson, G.M.B., 1956. Origin and distribution of the polyatomic molecules in the atmosphere. Proc. R. Soc. London. Ser. A. Math. Phys. Sci. 236, 187–193. https://doi.org/10.1098/rspa.1956.0127

Engel, A., Bönisch, H., Ullrich, M., Sitals, R., Membrive, O., Danis, F., Crevoisier, C., 2017. Mean age of stratospheric air

derived from AirCore observations. Atmos. Chem. Phys. 17, 6825–6838. https://doi.org/10.5194/acp-17-6825-2017

Engel, A., Möbius, T., Bönisch, H., Schmidt, U., Heinz, R., Levin, I., Atlas, E., Aoki, S., Nakazawa, T., Sugawara, S., Moore, F., Hurst, D., Elkins, J., Schauffler, S., Andrews, A., Boering, K., 2009. Age of stratospheric air unchanged within uncertainties over the past 30 years. Nat. Geosci. 2, 28–31. https://doi.org/10.1038/ngeo388

Flury, T., Wu, D.L., Read, W.G., 2013. Variability in the speed of the Brewer-Dobson circulation as observed by Aura/MLS. Atmos. Chem. Phys. 13, 4563–4575. https://doi.org/10.5194/acp-13-4563-2013

Fowler, D., Coyle, M., Skiba, U., Sutton, M.A., Cape, J.N., Reis, S., Sheppard, L.J., Jenkins, A., Grizzetti, B., Galloway, J.N., Vitousek, P., Leach, A., Bouwman, A.F., Butterbach-Bahl, K., Dentener, F., Stevenson, D., Amann, M., Voss, M., 2013. The global nitrogen cycle in the Twentyfirst century. Philos. Trans. R. Soc. B Biol. Sci. 368. https://doi.org/10.1098/rstb.2013.0164

Glückauf, E., 1944. A simple analysis of the helium content of air. Trans. Faraday Soc. 44, 436–439.

Graven, H.D., Guilderson, T.P., Keeling, R.F., 2012. Observations of radiocarbon in CO_2 at La Jolla, California, USA 1992-2007: Analysis of the long-term trend. J. Geophys. Res. Atmos. 117, 1–14. https://doi.org/10.1029/2011JD016533

Haenel, F.J., Stiller, G.P., Von Clarmann, T., Funke, B., Eckert, E., Glatthor, N., Grabowski, U., Kellmann, S., Kiefer, M., Linden, A., Reddmann, T., 2015. Reassessment of MIPAS age of air trends and variability. Atmos. Chem. Phys. 15, 13161–13176. https://doi.org/10.5194/acp-15-13161-2015

Hamilton, K., Fan, S.-M., 2000. Effects of the stratospheric quasi-biennial oscillation on long-lived greenhouse gases in the troposphere. J. Geophys. Res. 105, 20581. https://doi.org/10.1029/2000JD900331

Hamme, R.C., Emerson, S.R., 2004. The solubility of neon, nirogen and argon in distilled water and seawater. Deep. Res. I 51, 1517–1528.

Hegglin, M.I., Shepherd, T.G., 2009. Large climate-induced changes in ultraviolet index and stratosphere-to- troposphere ozone flux. Nat. Geosci. 2, 687–691. https://doi.org/10.1038/ngeo604

Henneberg, D., Heinrichs, U., Schomburg, G., 1975. Open Split Connection of Glass Capillary Columns to Mass Spectrometers. Chromatographia 8, 449–451.

Holland, P.W., Emerson, D.E., 1987. A determination of the helium 4 content of near-surface atmospheric air within the continental United States. J. Geophys. Res. Solid Earth 92, 12557–12566.

Holton, J.R., Haynes, P.H., Mcintyre, M.E., Douglass, A.R., Rood, B., 1995. Stratosphere-Troposphere. Rev. Geophys. 403–439.

Ishidoya, S., Sugawara, S., Inai, Y., Morimoto, S., Honda, H., Ikeda, C., Hashida, G., Machida, T., Tomikawa, Y., Toyoda, S., Goto, D., Aoki, S., Nakazawa, T., 2018. Gravitational separation of the stratospheric air over Syowa, Antarctica and its connection with meteorological fields. Atmos. Sci. Lett. 19, 1–7. https://doi.org/10.1002/asl.857

Ishidoya, S., Sugawara, S., Morimoto, S., Aoki, S., Nakazawa, T., 2008. Gravitational separation of major atmospheric components of nitrogen and oxygen in the stratosphere. Geophys. Res. Lett. 35. https://doi.org/10.1029/2007GL030456

Ishidoya, S., Sugawara, S., Morimoto, S., Aoki, S., Nakazawa, T., Honda, H., Murayama, S., 2013. Gravitational separation

in the stratosphere - A new indicator of atmospheric circulation. Atmos. Chem. Phys. 13, 8787–8796. https://doi.org/10.5194/acp-13-8787-2013

Ishidoya, S., Sugawara, S., Tohjima, Y., Goto, D., Ishijima, K., Niwa, Y., Aoki, N., Murayama, S., 2020. Secular change of the atmospheric Ar/N_2 and its implications for ocean heat uptake and Brewer-Dobson circulation. Atmos. Chem. Phys. Discuss. https://doi.org/doi.org/10.5194/acp-2020-301

Jenkins, W.J., Lott, D.E., Cahill, K.L., 2019. A determination of atmospheric helium, neon, argon, krypton, and xenon solubility concentrations in water and seawater. Mar. Chem. 211, 94–107. https://doi.org/10.1016/j.marchem.2019.03.007

Keeling, R.F., 1988. Development of an interferometric oxygen analyzer for precise measurement of the atmospheric O_2 mole fraction. Harvard University.

Keeling, R.F., Blaine, T., Paplawsky, B., Katz, L., Atwood, C., Brockwell, T., 2004. Measurement of changes in atmospheric Ar/N_2 ratio using a rapid-switching, single-capillary mass spectrometer system. Tellus 56B, 322–338. https://doi.org/10.1111/j.1600-0889.2004.00117.x

Keeling, R.F., Manning, A.C., McEvoy, E.M., Shertz, S.R., 1998. Methods for measuring changes in atmospheric O_2 concentration and their application in southern hemisphere air. J. Geophys. Res. 103, 3381–3397. https://doi.org/10.1029/97JD02537

Keeling, R.F., Manning, A.C., Paplawsky, W.J., Cox, A.C., 2007. On the long-term stability of reference gases for atmospheric O_2/N_2 and CO_2 measurements. Tellus B Chem. Phys. Meteorol. 59B, 3–14. https://doi.org/10.1111/j.1600-0889.2006.00196.x

Kockarts, G., 1973. Helium in the terrestrial atmosphere. Space Sci. Rev. 14, 723–757. https://doi.org/10.1007/BF00224775

Li, F., Waugh, D.W., Douglass, A.R., Newman, P.A., Pawson, S., Stolarski, R.S., Strahan, S.E., Nielsen, J.E., 2012. Seasonal variations of stratospheric age spectra in the Goddard Earth Observing System Chemistry Climate Model (GEOSCCM). J. Geophys. Res. Atmos. 117, 1–14. https://doi.org/10.1029/2011JD016877

Lupton, J., Evans, L., 2013. Changes in the atmospheric helium isotope ratio over the past 40 years. Geophys. Res. Lett. 40, 6271–6275. https://doi.org/10.1002/2013GL057681

Lupton, J., Evans, L., 2004. The atmospheric helium isotope ratio: Is it changing? Geophys. Res. Lett. 31, 1–4. https://doi.org/10.1029/2004GL020041

Mabry, J.C., Lan, T., Boucher, C., Burnard, P.G., Brennwald, M.S., Langenfelds, R., Marty, B., 2015. No evidence for change of the atmospheric helium isotope composition since 1978 from re-analysis of the Cape Grim Air Archive. Earth Planet. Sci. Lett. 428, 134–138. https://doi.org/10.1016/j.epsl.2015.07.035

Montzka, S.A., Dutton, G.S., Yu, P., Ray, E., Portmann, R.W., Daniel, J.S., Kuijpers, L., Hall, B.D., Mondeel, D., Siso, C., Nance, J.D., Rigby, M., Manning, A.J., Hu, L., Moore, F., Miller, B.R., Elkins, J.W., 2018. An unexpected and persistent increase in global emissions of ozone-depleting CFC-11. Nature 557, 413–417. https://doi.org/10.1038/s41586-018-0106-2

Nevison, C.D., Dlugokencky, E., Dutton, G., Elkins, J.W., Fraser, P., Hall, B., Krummel, P.B., Langenfelds, R.L., O'Doherty, S., Prinn, R.G., Steele, L.P., Weiss, R.F., 2011. Exploring causes of interannual variability in the seasonal cycles of tropospheric nitrous oxide. Atmos. Chem. Phys. 11, 3713–3730. https://doi.org/10.5194/acp-11-3713-2011

Oliver, B.M., Bradley, J.G., Farrar IV, H., 1984. Helium concentration in the Earth's lower atmosphere. Geochim. Cosmochim. Acta 48, 1759–1767. https://doi.org/10.1016/0016-7037(84)90030-9

Pierson-Wickmann, A.C., Marty, B., Ploquin, A., 2001. Helium trapped in historical slags: A search for temporal variation of the He isotopic composition of air. Earth Planet. Sci. Lett. 194, 165–175. https://doi.org/10.1016/S0012-821X(01)00554-4

Ray, E.A., Moore, F.L., Rosenlof, K.H., Davis, S.M., Boenisch, H., Morgenstern, O., Smale, D., Rozanov, E., Hegglin, M., Pitari, G., Mancini, E., Braesicke, P., Butchart, N., Hardiman, S., Li, F., Shibata, K., Plummer, D.A., 2010. Evidence for changes in stratospheric transport and mixing over the past three decades based on multiple data sets and tropical leaky pipe analysis. J. Geophys. Res. Atmos. 115, 1–16. https://doi.org/10.1029/2010JD014206

Ray, E.A., Moore, F.L., Rosenlof, K.H., Davis, S.M., Sweeney, C., Tans, P., Wang, T., Elkins, J.W., Bönisch, H., Engel, A., Sugawara, S., Nakazawa, T., Aoki, S., 2014. Improving stratospheric transport trend analysis based on SF_6 and CO_2 measurements. J. Geophys. Res. Atmos. 119, 14110–14128. https://doi.org/10.1002/2014JD021802

Reid, R.C., Prausnitz, J.M., Poling, B.E., 1987. The properties of gases and liquids, 4th ed. McGraw-Hill, New York.

Salby, M.L., Callaghan, P.F., 2006. Influence of the Brewer-Dobson circulation on stratosphere-troposphere exchange. J. Geophys. Res. Atmos. 111, 1–9. https://doi.org/10.1029/2006JD007051

Sano, Y., Furukawa, Y., Takahata, N., 2010. Atmospheric helium isotope ratio: Possible temporal and spatial variations. Geochim. Cosmochim. Acta 74, 4893–4901. https://doi.org/10.1016/j.gca.2010.06.003

Sano, Y., Marty, B., Burnard, P., 2013. Noble Gases in the Atmosphere, in: Burnard, P. (Ed.), The Noble Gases as Geochemical Tracers. Springer Berlin Heidelberg, pp. 17–31. https://doi.org/10.1007/978-3-642-28836-4_2

Sano, Y., Wakita, H., Makide, Y., Tominaga, T., 1989. A ten-year decrease in the atmospheric helium isotope ratio possibly caused by human activity. Geophys. Res. Lett. 16, 1371–1374. https://doi.org/10.1029/GL016i012p01371

Simmonds, P.G., Manning, A.J., Athanassiadou, M., Scaife, A.A., Derwent, R.G., O'Doherty, S., Harth, C.M., Weiss, R.F., Dutton, G.S., Hall, B.D., Sweeney, C., Elkins, J.W., 2013. Interannual fluctuations in the seasonal cycle of nitrous oxide and chlorofluorocarbons due to the Brewer-Dobson circulation. J. Geophys. Res. Atmos. 118, 10694–10706. https://doi.org/10.1002/jgrd.50832

Sugawara, S., Ishidoya, S., Aoki, S., Morimoto, S., Nakazawa, T., Toyoda, S., Inai, Y., Hasebe, F., Ikeda, C., Honda, H., Goto, D., Putri, F.A., 2018. Age and gravitational separation of the stratospheric air over Indonesia. Atmos. Chem. Phys. 18, 1819–1833. https://doi.org/10.5194/acp-18-1819-2018

Torgersen, T., 1989. Terrestrial helium degassing fluxes and the atmospheric helium budget: Implications with respect to the degassing processes of continental crust. Chem. Geol. Isot. Geosci. Sect. 79, 1–14. https://doi.org/10.1016/0168-9622(89)90002-X

Weiss, R.F., 1971. Solubility of helium and neon in water and seawater. J. Chem. Eng. Data 16, 235–241. https://doi.org/10.1021/je60049a019

Zartman, R.E., Wasserburg, G.J., Reynolds, J.H., 1961. Helium, Argon, and Carbon in Some Natural Gases. J. Geophys. Res. 66, 277–306. https://doi.org/10.1029/jz066i001p00277

11 Figures and Figure Captions

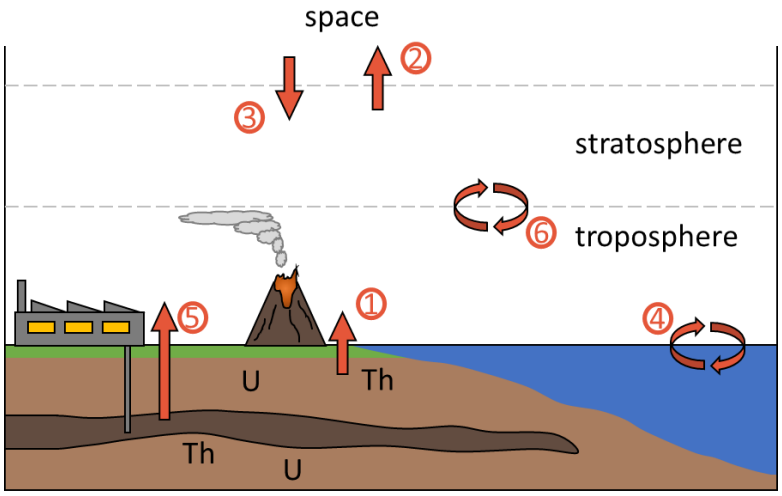

Figure 1. Schematic depiction of ^{4}He fluxes to and from the troposphere. Different processes are numbered and listed in Table 1.

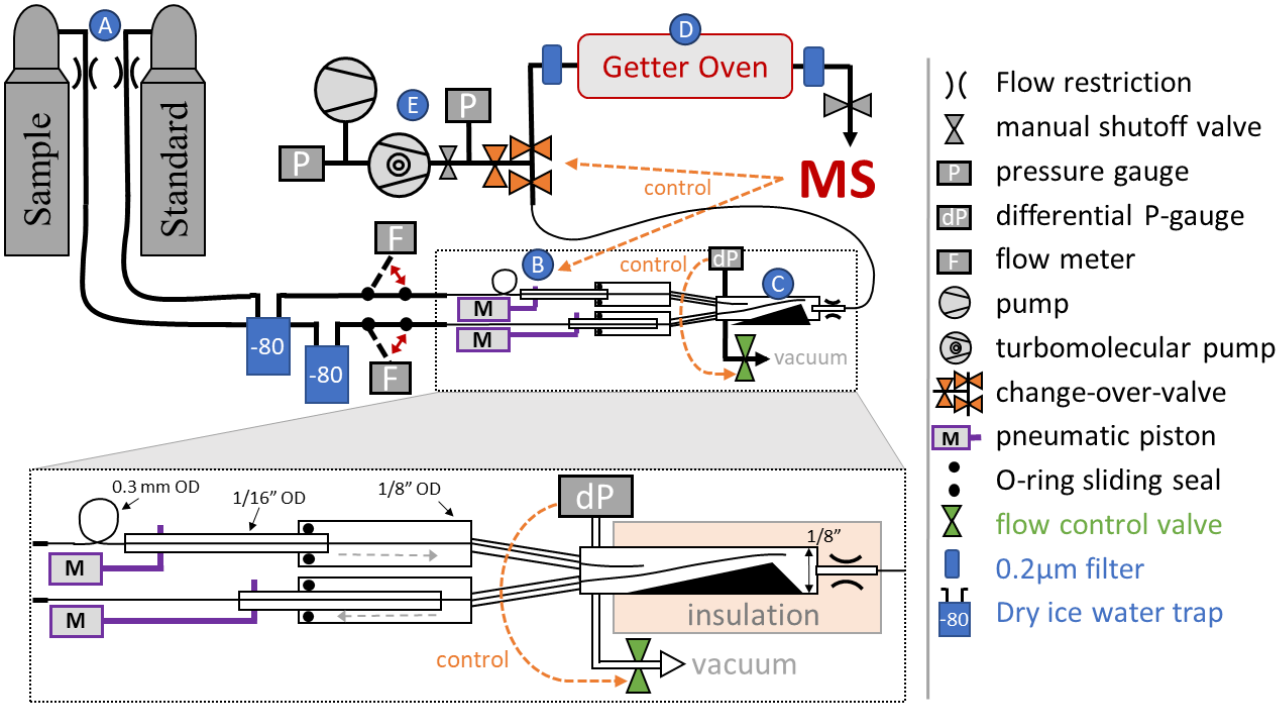

Figure 2. Schematic depiction of the flow-stabilizing MS inlet system. Dashed orange arrows highlight important control pathways and letters A-E in blue circles label the main sections of the inlet system. Red double arrows indicate manual switching option in the inlet system. Sample or standard gas is delivered from high-pressure cylinders (A). The flow can be measured by two Omron flow meters before entry into the pressure stabilization chamber (C). Pistons (B) alternately move fine metal tubing in the pressure stabilization chamber, pushing either the sample or standard gas stream deeper into the stabilization chamber where the gas will be picked up by a single capillary leading to the MS. A sliding seal is made using lubricated O-rings between 1/8" and 1/16" OD tubing at the entry to the pressure-stabilized chamber. This ensures sufficient rigidity and protects the fine metal tubing inside The chamber is exhausted to a vacuum system and the pressure is monitored and controlled by a differential pressure gauge combined with an automatic MKS flow control valve. The stainless-steel getter oven (D) has an inner diameter of 1/2" and is filled with 10–12 g of titanium sponge. 2µm-filters prevent particles from contaminating the MS and gas delivery system. In case of an anomalous pressure change in the MS or when venting the getter oven, the getter oven can be isolated from the pressure-stabilization chamber with a change-over-valve controlled directly by the MS software. The entire inlet vacuum system is backed by a diaphragm vacuum pump and a turbomolecular pump (E). A manual shutoff-valve can isolate the getter oven from the MS.

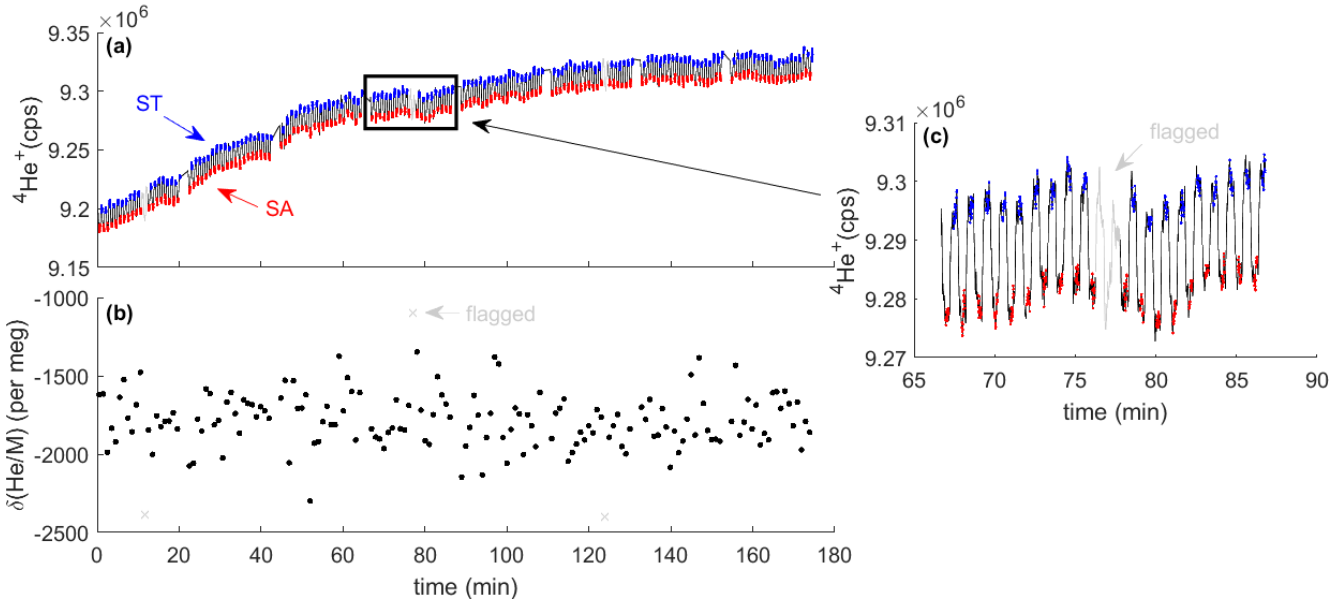

480 **Figure 3.** Typical analysis results from the measurement of two high pressure cylinders. The MS monitors the $^4He^+$-ion beam during switching between sample (SA) and standard (ST) gas (a). Red and blue shaded data points highlight the periods used for integration and calculation of the delta value (b). They are separated by idle times (black lines) to allow complete flushout after switching. Data are quality controlled and flagged periods are shown in grey. Inset (c) shows one block of 20 sample-standard comparisons including one pair of cycles that was flagged as an outlier.

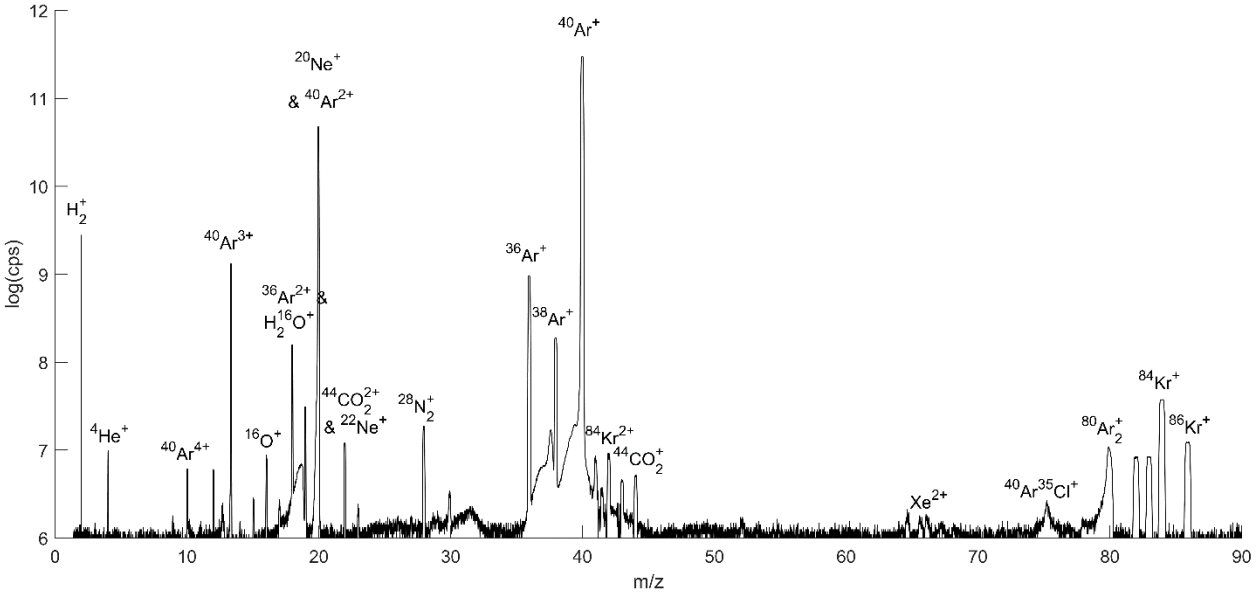

485

Figure 4. Mass scan of ambient air. Ion beam intensity is shown as the logarithm of the ions counted per second, and select ion species are labeled.

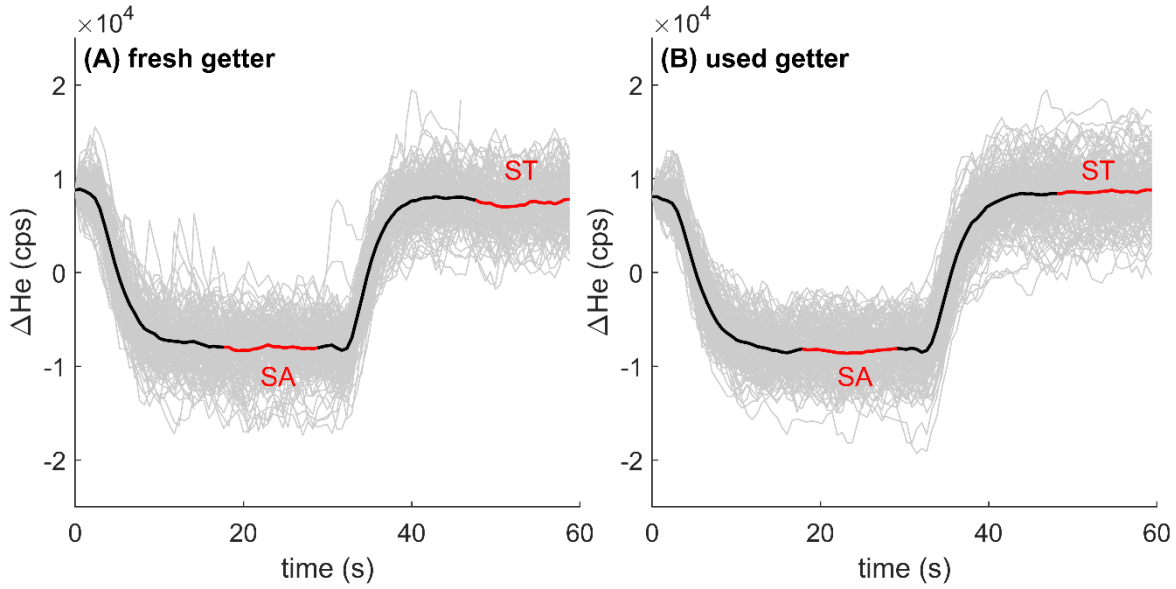

Figure 5. Stack of ^{4}He ion count difference (10^4 counts per second, cps) when switching between the same standard (ST) and sample (SA) gas stream using fresh titanium sponge (A) and nearly depleted getter material (B). Grey lines show individual records forced to align at time equals zero, and the thick black line shows the average of all stacked switching events. The analysis cycle consists of (i) switching to SA with an idle time of ~18 seconds, (ii) a ~12 second integration of ions from SA, (iii) switching back to ST, again with a ~18 second idle time, and finally (iiii) a ~12 second integration of ST.

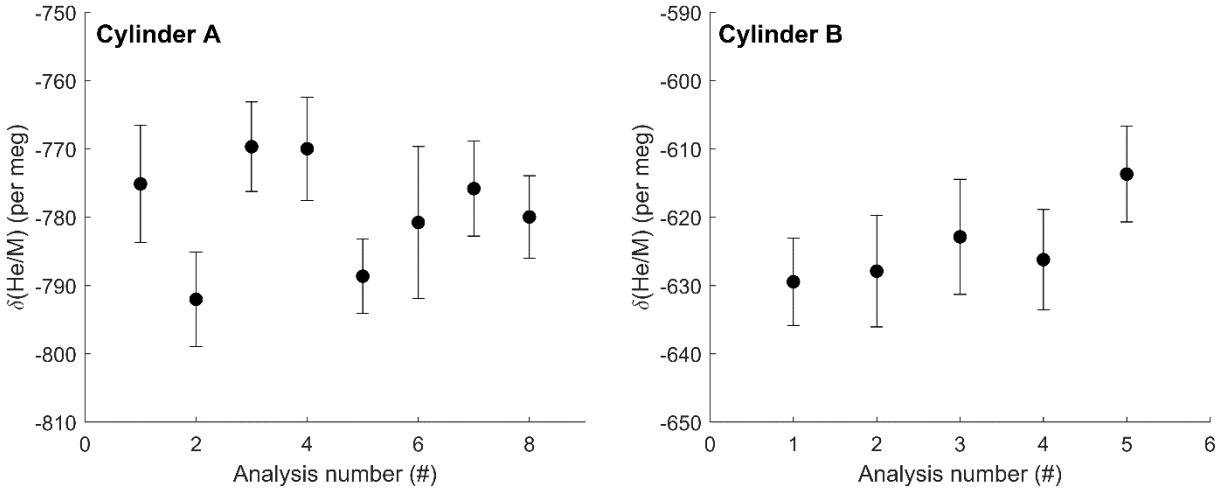

Figure 6. Repeat δ(He/M) analysis of two high-pressure cylinders against ambient La Jolla air collected in 2019. Each data point shown is the average of at least 300 individual 12-sec measurements with 1σ error bars representing the standard error of each measurement. Repeat analyses show a standard deviation of 8.1 and 6.3 per meg (1σ) for cylinder A and cylinder B respectively. Analysis 6 for cylinder A was shorter resulting in a larger uncertainty for that measurement. Data are not corrected for zero enrichment effects discussed in the text.

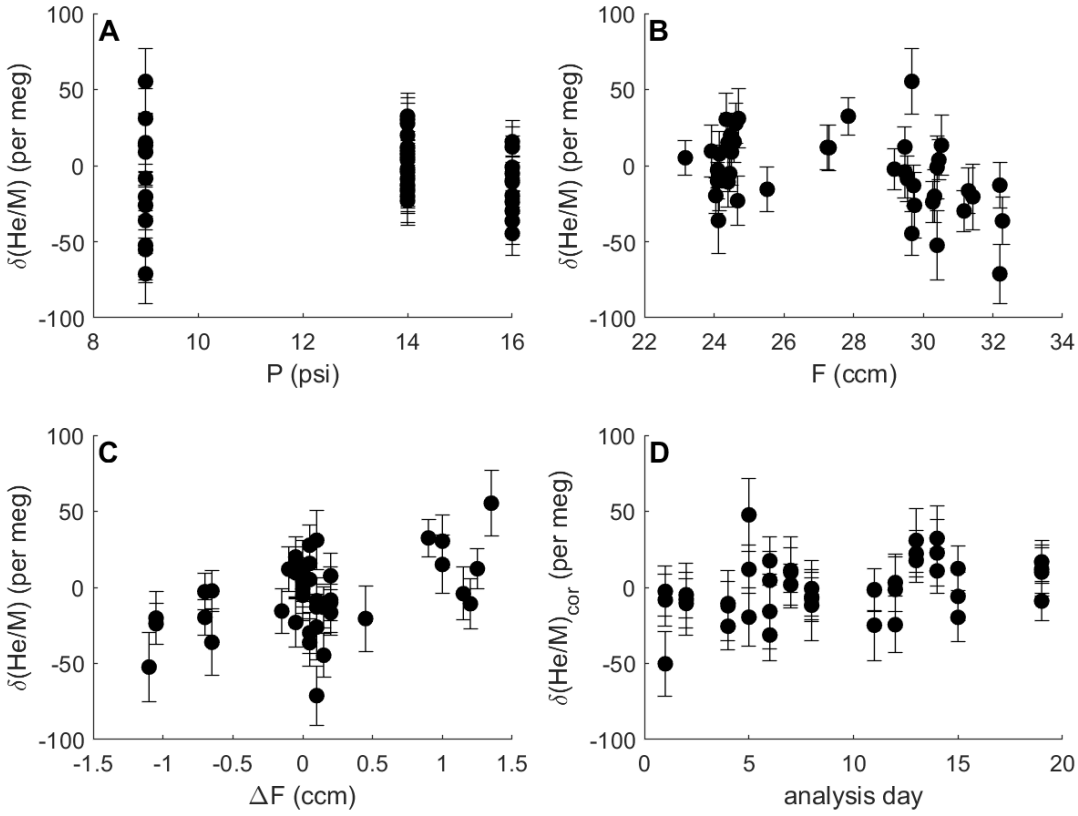

Figure 7. Difference in δ(He/M) between two identical gas streams (i.e., the zero enrichment) measured repeatedly under different conditions over 1.5–3h. Error bars show 1σ uncertainty (internal precision). Measurements were made at different pressure levels (a), with slightly varying gas flows to the stabilization chamber (b), and imbalances in flow between SA and ST side (c). The same shared capillary was used for all analysis. Therefore, the pressure in the stabilization chamber controls the intensity of the ion beam and the internal precision of the analysis, illustrated by the greater scatter of observations at 9 psi (62.1 kPa). Delta values shown in (d) were corrected for the influence of pressure, mean flow, and flow imbalance according to coefficients found by multiple linear regression (see text). For a pressure of 14 psi (96.5 kPa), corrected delta values generally show scatter as expected from shot-noise behavior and corrected delta values are stable over time.

12 Tables and Table Captions

Table 1. Processes contributing to variations in the tropospheric and stratospheric $^4He/N_2$ ratio.

Process	^4He flux (10^7 mol y^{-1})	$\delta(^4He/N_2)$ trend[1] (per meg y^{-1})	$\delta(^4He/N_2)$ anomaly (per meg)	References
Long-term tropospheric changes				
(1) Crustal degassing and volcanism	24.0–50.7	0.26–0.55		(Torgersen, 1989)
(2) Loss to space	53.3–106.8	-0.58–-1.15		(Kockarts, 1973; Torgersen, 1989)
(3) Non-terrestrial sources	insignificant	-		(Torgersen, 1989)
(4) Global Ocean warming[2]	1.3	-0.16		
(5) Fossil fuel extraction[3]	3189–12755 13000±7000 34000	34–138 140±76 367		(Oliver et al., 1984) (Pierson-Wickmann et al., 2001) (Sano et al., 2013)
(6) BDC acceleration[4]		0.5		
Long-term stratospheric changes				
BDC acceleration[4]		-15		
Observational constraints on tropospheric trends[5]		-1.4±44.5 9.5±32.7 -2±23.8		(Lupton and Evans, 2013) (Mabry et al., 2015) (Boucher et al., 2018c)
Short-term and spatial variability				
Seasonal cycle of global ocean heat[6]			±1.5–4.5	
Strat. circ. & STE variability signal[7] -troposphere -stratosphere			 ±3 ±187.5	
Interhemispheric difference[9]			<30	

[1] $\delta(^4He/N_2)$ trends are calculated using first column and assuming total atmospheric ^4He = 9.268e+14 mol. N_2 changes are generally neglected except for ocean degassing. Tropospheric trends are globally uniform because the troposphere is well mixed. Stratospheric trend estimates are given for 35km in the mid latitude Northern Hemisphere.

[2] calculated from ^4He and N_2 solubility changes (Hamme and Emerson, 2004; Weiss, 1971) for an ocean heat content trend of 10ZJ y^{-1} at a mean water temperature of 10°C.

[3] (i) includes natural gas, coal and uranium, (ii) and (iii) include natural gas, petroleum and coal.

[4] $\delta(^4He/N_2)$ rescaled from $\delta(Ar/N_2)$ assuming 7.5x greater gravitational separation. The secular $\delta(Ar/N_2)$ trend was simulated in the SOCRATES model for an accelerating BDC scenario (+4 % dec^{-1}) by Ishidoya et al. (2020). $\delta(^4He/N_2)$ trend is adjusted to reflect a more plausible BDC acceleration of +2 % dec^{-1}.

[5] observed $^3He/^4He$ trends are translated to $^4He/N_2$ trends assuming $^3He/^4He$ = 3e-8 for fossil fuel associated helium (Sano et al., 2013).

[6] scaled from seasonal $\delta(Ar/N_2)$ changes of 5-15 per meg (Keeling et al., 2004) using solubility-temperature dependency of He, N_2 and Ar in a 10°C warm surface ocean (Hamme and Emerson, 2004; Weiss, 1971).

[7] Tropospheric and stratospheric $\delta(^4He/N_2)$ rescaled from $\delta(Ar/N_2)$. Ishidoya et al. (2020) report a ±0.4 and ±25 per meg $\delta(Ar/N_2)$ change in troposphere and stratosphere in the SOCRATES model for a sinusoidal ±5% change in BDC strength over 3 years.

[8] Assuming that industrial He release is confined to the Northern Hemisphere and assuming an annual $\delta(^4He/N_2)$ increase of ~30 per meg (consistent with the current observational error) yields an interhemispheric $\delta(^4He/N_2)$ difference < 30 per meg. Differences in STE of He between the hemispheres are neglected here but could be important.

Table 2. Summary of observed ion beams in Figure 4. Relative ion beam intensities on MAT253 are calculated from the scan with identical source tuning. Xe isotope beams were not observed but scaled from previous observations in the lab.

m/z	Dominant ions	Ion beam intensity (cps)*	ion beam intensity relative to He^+
4	$^{4}He^{+}$	9.70E+06	1
20	$^{20}Ne^{+}$,$^{40}Ar^{2+}$	4.78E+10	4916.1
22	$^{22}Ne^{+}$,$^{44}CO_2^{2+}$	1.22E+07	1.25
36	$^{36}Ar^{+}$	9.55E+08	98.26
38	$^{38}Ar^{+}$	1.89E+08	19.44
40	$^{40}Ar^{+}$	2.98E+11	30660
82	$^{82}Kr^{+}$	8.50E+06	0.87
83	$^{83}Kr^{+}$	8.40E+06	0.86
84	$^{84}Kr^{+}$	3.76E+07	3.87
86	$^{86}Kr^{+}$	1.22E+07	1.25
129*	$^{129}Xe^{+}$	2.60E+06	0.27
131*	$^{131}Xe^{+}$	2.10E+06	0.22
132*	$^{132}Xe^{+}$	2.70E+06	0.28
136*	$^{136}Xe^{+}$	9.00E+05	0.09

*Xe isotopes were not measured directly here because of the limited dynamic range of the MAT 253 when set to measure He. Instead we report expected Xe ion beam intensities that were calculated using Kr ion beam intensities from this experiment and relative ion beam yields of Kr and Xe determined on a sperate MAT 253 in the lab.